*American Mineralogist, Volume 83, pages 685–699, 1998*

# Multicomponent diffusion in the molten system $K_2O$-$Na_2O$-$Al_2O_3$-$SiO_2$-$H_2O$

**JAMES E. MUNGALL,[1,2,*] CLAUDIA ROMANO,[1,3] AND DONALD B. DINGWELL[1]**

[1]Bayerisches Geoinstitut, Universität Bayreuth D-95440, Germany
[2]Ixion Research, 5475 Royalmount, no. 133, Montreal, Quebec H4P 1J3, Canada
[3]Universitá degli Studi di Roma 3, Departmento di Scienze della terra, L.go San Murialdo 1, Rome, Italy

## ABSTRACT

We have measured multicomponent chemical diffusion coefficients in a melt near to the low pressure water-saturated eutectic granite composition in the system $K_2O$-$Na_2O$-$Al_2O_3$-$SiO_2$-$H_2O$ at 1.0 GPa and temperatures of 1300 and 1600 °C. The measured diffusion profiles can be accounted for within the analytical error by diffusion coefficients, which are not dependent on composition within the range of compositions accessed by our experiments. The multicomponent diffusion coefficient matrix [*D*] has a highly degenerate set of real, positive eigenvalues that show a regular relation to melt viscosity on an Arrhenius diagram. The smallest eigenvalue is that associated predominantly with Si-Al exchange. The larger two eigenvalues are those associated with Si-Na and Si-K exchange and are effectively degenerate, with the result that exchanges of alkalis for silica or for each other can proceed in pseudo-binary fashion without inducing fluxes of other components. The eigenvalue associated with H-Si exchange is smaller than the alkali-silica eigenvalues, but analytical uncertainties make it also effectively degenerate with the alkalis. Uphill diffusion, notably of water and alkalis, was observed in several experiments, and this would lead to transient partitioning of water and alkalis across diffusion interfaces showing large $Al_2O_3$ concentration gradients. Such partitioning in natural systems would persist until Al concentration gradients were erased by continued, much slower Al-Si interdiffusion.

## INTRODUCTION

The province of igneous petrology is primarily the study of magmatic processes within and on the surface of the Earth. Quantitative descriptions of the physical chemistry of these processes have tended to rely on equilibrium thermodynamics (e.g., Ghiorso 1987a). Time-dependent processes therefore must be modeled as a series of discrete time steps, during each of which a system is assumed to be in a state of equilibrium. Because the assumption of thermodynamic equilibrium requires that not only the fastest, but also all time-dependent processes go to completion, it can commonly fail to account for compositions and textures observed in natural geological systems wherein no observable physical state represents a state of true closed-system equilibrium. In particular, situations in which some but not all processes go to completion can lead to serious errors if equilibrium is assumed. It is important to understand the ways that the processes themselves affect the predictions of the idealized equilibrium thermodynamics to which most of our present knowledge pertains and to understand how these rates of these processes can be described in the context of thermodynamic theory. For example, nucleation and growth of crystals from a melt result from a change in one of the state variables of a melt system that initially may have been close to equilibrium (Ghiorso 1987b). Chemical potential and temperature gradients drive the irreversible fluxes of chemical components and heat, both toward and away from the crystal-melt interface. The study of the thermodynamics of crystal growth therefore must include a theory of the thermodynamics of irreversible processes and, by similar arguments, we would suggest that a quantitative thermodynamic description of a magmatic system is not complete unless it includes a quantitative description of all of the irreversible processes that can occur within that system. Macroscopic processes whose rates, mechanisms, and final compositional states depend in part on the irreversible process of chemical diffusion include crystal growth (Ghiorso 1987b), magma degassing (Sparks et al. 1994), magma mixing, and gravitational instability in liquid interfaces (Trial and Spera 1990).

Despite the fact that a vast literature exists devoted to the quantitative description of irreversible (non-equilibrium) thermodynamics (e.g., Haase 1990; Kuiken 1994) and to potential applications of these principles to systems of geological interest (Allègre et al. 1981; Lasaga 1982; Fisher and Lasaga 1983; Kirkpatrick 1983; Ghiorso 1987b; Toramaru 1991; Richter 1993; Trial and Spera 1994), large gaps remain in the application of these prin-

* E-mail: mungall@cygnus.qc.ca

0003–004X/98/0708–0685$05.00

ciples to geology, particularly in the realm of experimental petrology. In recent years, several papers have addressed the application of irreversible thermodynamics to thermal diffusion in natural melts (Ghiorso 1987b; Lesher and Walker 1991) and to multicomponent diffusion in simple systems of three or four components (Kubicki et al. 1990; Kress and Ghiorso 1993; Liang et al. 1996; Chakraborty et al. 1995a, 1995b). Only one study has addressed multicomponent diffusion in a natural basaltic composition, but it did not treat diffusion of all of the components present in the melt (Kress and Ghiorso 1995). Numerous studies have described diffusion in natural systems and synthetic analogs (see reviews by Hofman 1980 and Chakraborty 1995), almost exclusively in the form of tracer or self-diffusion coefficients, or as pseudo-binary chemical diffusivities that generally cannot be applied to systems outside the specific ones in which they were measured. Until now, no experimental study has been published that provides a complete quantitative thermodynamic description of chemical diffusion in a multicomponent melt of direct geological relevance.

We therefore began an investigation of chemical diffusion processes in a synthetic melt system having enough chemical components to be considered a realistic analog to natural magmas. We chose a five-component base composition that lies near the water-saturated, low-pressure eutectic in the system $K_2O$-$Na_2O$-$Al_2O_3$-$SiO_2$-$H_2O$ (Tuttle and Bowen 1958). In this paper, we describe the results of experiments aimed at deriving a quantitative, predictive model for multicomponent diffusion in melts near the base composition at elevated temperatures (1300 °C and 1600 °C) and pressure (1.0 GPa).

## Multicomponent diffusion

### Background

The general principles necessary for a quantitative macroscopic description of chemical diffusion in multicomponent melts are well-described elsewhere (e.g., Gupta and Cooper 1971; Kuiken 1994), and we refer the interested reader to these other works. The multicomponent form of Fick's first law for a system with $n$ chemical components in one-dimensional system (all fluxes and thermodynamic forces in a single direction in space) is our starting point:

$$\overline{J} = -\rho[D]\frac{\partial \overline{x}}{\partial y} \tag{1}$$

(See Table 1 for notation). Equation 1 is actually a series of $(n - 1)$ equations:

$$J_k = -\rho\sum_{l=1}^{n-1} D_{kl}\frac{\partial x_l}{\partial y} \tag{2}$$

which express that the flux of each component depends linearly through the $D_{kl}$ on the concentration gradients of each of the other independent components. We assume implicitly that the melt components all have the same partial molar density, an assumption that simplifies the ensuing calculations with minimal loss of accuracy provided that we are interested in the molar fluxes rather than density distributions in the interfacial region. The flux and concentration of the $n^{th}$ component is dependent on those of the other $(n - 1)$ components through closure. Equation 2 allows for chemical diffusion of a component up its own concentration gradient (uphill diffusion) for cases when:

$$D_{kk}\frac{\partial x_k}{\partial y} < \sum_{l=1}^{n-1} D_{kl}\frac{\partial x_l}{\partial y}, \qquad k \neq l \tag{3}$$

To derive useful information from Equation 1, we seek analytical solutions giving $x$ as a function of time and space; the detailed derivation of useful analytical solutions of Equation 1 appears in the Appendix.

### Methods of solving for [$D$] from experimental data

The model equation, A12, permits us to determine the values of [$D$] from experimentally measured profiles of concentration, $\overline{c}_{(y,t)}$. Data can be gathered in several ways, but the usual approach to the study of diffusion in silicate melts is to quench the experimental sample to a glass and prepare a polished section along a plane cut parallel to its length. This section then can be studied by techniques such as electron microprobe analysis (EMPA) or secondary ion mass spectrometry (SIMS) to yield empirical values of $\overline{c}_{(y,t)}$.

If a diffusion couple is chosen that is parallel to an eigenvector in composition space, then the couple behaves as a binary system and only information regarding that eigenvector and its eigenvalue can be gleaned from the diffusion profiles. Trial and Spera (1994) state that if a diffusion profile appears pseudo-binary then it must lie along an eigenvector. However, in the case where two or more eigenvalues are equal within measurement error, couples in all directions within a plane containing both eigenvectors will have diffusion profiles that appear binary. In this case, there are repeated roots of the polynomial in Equation A4 and the eigenvectors cannot be defined uniquely. One can then choose any convenient pair of eigenvectors within the plane for modeling purposes. Consequently, systems with degenerate eigenvalues cannot be used to calculate a unique [$D$] and only the eigenvalues themselves have any meaning as diffusion coefficients. If the couple does not parallel an eigenvector and the eigenvalues are not identical, then the diffusion profiles created within even a single couple, in principle, should contain sufficient information to constrain [$D$]. However, as Trial and Spera (1994) have shown, imprecision in the analytical data results in enormous uncertainties in [$D$] matrices that are extracted from single couples. To be sure that information is obtained on all the eigenvectors and eigenvalues belonging to [$D$], the experimentalist should carry out at least $(n - 1)$ couple experiments in a system of $(n - 1)$ independent components, such that the orientation of couples in composition space is as orthogonal as possible (Trial and Spera 1994).

The values of the diffusion coefficients must be esti-

mated by comparing the model equation, A12, with the experimental data. We cannot implement standard inverse error function models without first knowing the orientations of the eigenvectors with which [*D*] must be decoupled to give binary interdiffusion profiles. Consequently, we are forced to use a forward-modeling approach. In a forward model, we propose an initial form for [*D*] and then solve Equation A12 for the appropriate boundary conditions and experiment durations. The resulting model diffusion profiles are then compared with the actual data using a merit function such as $\chi^2$:

$$\chi^2 = \sum_{l=1}^{m} \sum_{k=1}^{n} \left( \frac{c_k(y_l, t_l) - x_k(\overline{a}; y_l, t_l)}{\sigma_{kl}} \right)^2 \qquad (4)$$

where $c_k$ is the measured mole fraction, $x_k$ is the mole fraction of component $k$ predicted by the model Equation A12, and $\sigma_{kl}$ is the standard deviation in $c_k$ at position $l$. The vector $\overline{a}$ in Equation 4 is composed of all eigenvector elements and eigenvalues combined into one. The challenge in the forward-modeling approach is to find a way to improve iteratively the quality of the fit to the data afforded by $\overline{a}$. Elegant numerical methods exist by which the convergence can be performed with a minimal amount of guidance from the investigator (e.g., Trial and Spera 1994; Kress and Ghiorso 1993, 1995). However, these methods require very time-consuming preparation of sophisticated computer codes. Much simpler, interactive approaches often can produce equally good results in less time, and give the investigator an appreciation of the significance of the various elements of [*P*] and [$\Lambda$] (see Appendix). Our approach begins with a computer program that implements Equation A12 and estimates goodness of fit for all available microprobe data in the system of interest for a single choice of $\overline{a}$. The code then optimizes individual $a_k$ one at a time, by determining $\chi^2$ at several values of $a_k$ distributed around its initial value. The value of $a_k$ yielding the smallest value of $\chi^2$ is chosen to replace the initial value, and the process is repeated for $a_{k+1}$. At the beginning of the process, $\overline{a}$ is seeded with elements that give [*P*] a simple structure (for example: $P_{kk} = 1.0$, $P_{kl} = 0.1$ for $k \neq l$). We have found, using this approach interactively, that a complete [*D*] for a five-component system can be optimized in a few hours by one person with a personal computer. Extension of the iterative forward-modeling approach to systems of more than five components should be straightforward.

### Estimation of errors

The parameters retrieved from the forward modeling described above have associated errors that are difficult to estimate by standard methods of error propagation. Trial and Spera (1994) describe the use of Monte Carlo simulations to find the uncertainties in the elements of [*D*], but this method is also cumbersome. Quantitative use of the [*D*] in modeling applications relies on the eigenvalues and eigenvectors through Equation A12. Degeneracy in the eigenvalues (see results section below) makes it impossible to calculate values for [*D*] even if we possess a set of eigenvalues and eigenvectors that describes multicomponent diffusion in a given system perfectly. In other words, the set of uncoupled diffusion coefficients represented by the eigenvalues is the only set of diffusion coefficients we can be sure of being able to use. Because we do not use the elements of [*D*] in quantitative applications, we leave the estimation of errors in the elements of [*D*] an open but largely irrelevant question, and focus on error estimation in the eigen-parameters themselves. We remind the reader that the eigenvalues of [*D*] are themselves the set of diffusion coefficients, which describe the diffusivities of the components defined by Equation A6.

A simple and very widely used means of estimating errors in fit parameters that have been determined through a $\chi^2$ analysis is suggested by Press et al. (1992, p. 688). If the best-fit solution to Equation 4 is the vector $\overline{a}_{(o)}$, then a confidence interval for each element of $\overline{a}_{(o)}$ can be assessed by determining the range of values for each $a_k$ within which the value of $\chi^2$ does not exceed a limiting value. For example, if the limiting change in $\chi^2$ is set at 1.0, considering only one parameter at a time, then the resulting interval is the 68.3% confidence interval. Similarly, the 90% confidence interval is bounded by the limits at which $\chi^2$ has increased by 2.71 (Press et al. 1992, p. 692). Covariances between elements of the solution array $\overline{a}_{(o)}$ may lead to deviations considerably greater than would be implied when confidence intervals on individual elements of $\overline{a}_{(o)}$ are considered. More elaborate methods of calculating confidence intervals set stringent requirements on the type of statistical distribution of the data around its mean. Because we do not know the type of distribution to expect in the elements of [*P*] and [$\Lambda$], we cannot justify their use.

## Experimental methods

The starting materials for our experiments were the same glasses used to measure water solubility in the haplogranite system by Holz et al. (1992) and to measure viscosities by Hess and Dingwell (1996a). The compositions measured at the ends of the experimental products are listed in Table 2. The glasses were prepared by fusing 100 g mixtures of oxide and carbonate powders for 2 h in a platinum crucible at 1600 °C to produce a bubble-rich slurry of melt and crystals. This material was stirred at 1600 °C for several days with a platinum spindle and then cooled in air. Preparation in this manner ensures that the highly viscous melt is homogeneous and free of crystals to at least the precision of electron microprobe analysis. For our experiments, these homogenous, bubble- and crystal-free glasses were crushed in an agate mortar and pestle to a grain size of 50 μm.

The powdered glass was then placed in cylindrical platinum capsules 5 mm in diameter and 11 mm long with 0.1 mm thick walls and hammered into place with hardened steel tools specially made to prevent deformation of the sample during pressing. The interface was tamped flat with a smooth steel tool before the second powder was

**TABLE 1.** Notation

| | |
|---|---|
| $\underline{a}$ | vector containing all elements of [$P$] and [$\Lambda$] in $\chi^2$ fitting |
| $\underline{c}$ | measured vector of mole fractions of chemical components |
| $\underline{C}$ | orientation of a diffusion couple in composition space. |
| $D^0$ | diffusion coefficient of network-forming cations (cm$^2$/s) |
| [$D$] | matrix of diffusion coefficients $D_{kl}$ (cm$^2$/s) |
| $erf()$ | error function |
| [$F$] | diagonal matrix of linear operators |
| $\underline{J}$ | vector of barycentric molar component fluxes (mol cm$^2$/s) |
| $k_B$ | Boltzmann's constant (1.3805 $\times$ 10$^{-23}$ J/K) |
| $L$ | length of one side of a diffusion couple (cm) |
| [$P$] | matrix whose columns are the eigenvectors of [$D$] |
| $t$ | time (s) |
| $\underline{T}$ | temperature (K) |
| $\underline{u}$ | transformed vector of mole fractions of chemical components |
| $\underline{x}$ | vector of mole fractions of chemical components |
| $y$ | distance (cm) |
| $\delta_{kl}$ | Kronecker delta equal to l for k = l, equal to 0 for all k $\neq$ 1 |
| $\epsilon_{H_2O,OH}$ | infrared absorptivity of water, OH radicals |
| $\eta$ | viscosity (Pa·s) |
| $\lambda^*$ | length scale associated with jump distance for diffusion (cm) |
| [$\Lambda$] | diagonal matrix of eigenvalues of [$D$] (cm$^2$/s) |
| $\underline{\lambda}$ | vector of eigenvalues $\lambda_k$ of [$D$] (cm$^2$/s) |
| $\underline{\nu}$ | eigenvector of [$D$] with ($n$ − 1) components |
| $\underline{\nu}^*$ | extended eigenvector of [$D$] with $n$ elements |
| $\rho$ | molar density of melt (mol/cm$^3$) |
| $\underline{\sigma}$ | standard deviation |
| $\underline{\chi}$ | composition of an end-member of a diffusion couple |

loaded in on top. The bases of the capsules were hammered out flat, whereas the tops were flat discs with upturned rims welded in place. Distilled water was added immediately before closing capsules. In our initial experiments, we made the assumption that the water would distribute itself uniformly throughout the capsule during heating, so that when the glass passed through its glass transition and trapped the water between coalescing particles of melt, the water concentration would be equal throughout the capsule. For some experiments this was found to be true, but in other cases the water was found to have been distributed non-uniformly. Consequently, we performed additional experiments in which starting materials were pre-hydrated in the piston cylinder by loading capsules with glass of uniform composition and water content, and holding them at 1600 °C and 1.0 GPa for at least 1 h. The products of these synthesis experiments were then ground as before and used as starting materials for diffusion couples. The consequences of non-uniform distributions of water for the retrieved diffusion coefficients of other components are negligible, as discussed below.

Our experiments were conducted in a ¾″ end-loaded piston-cylinder apparatus using methods previously described by Mungall and Dingwell (1997). All experiments were conducted at a nominal pressure of 1.0 GPa; the actual pressure varied by no more than 20%. Reported temperatures are accurate to within 20 °C, inclusive of the effects of thermal gradients through our long capsules (Mungall and Dingwell 1997). Temperatures were raised to conditions of the experiments at a rate of either 200 or 400 K/min. Experiments were heated through the final 10 °C over a period of about 1 min to prevent overshoot of the desired temperature. Experiments were quenched by turning off the furnace, giving cooling rates of approximately 200 K/s.

## Experimental conditions

We performed eight experiments along seven different diffusion couples (i.e., seven different pairs of end-member compositions) at 1600 °C and five experiments along four diffusion couples at 1300 °C (Table 2). Three couples (1, 2, and 4 in Table 2) lie parallel to the plane containing albite, orthoclase, and quartz (the haplogranite plane) in the system $K_2O$-$Na_2O$-$Al_2O_3$-$SiO_2$, but offset by 3 wt% $H_2O$, intersecting at the composition of HPG8 + 3 wt% $H_2O$ (Fig. 1). Two more couples (3 and 5 in Table 2) lie at high angles to this plane. Couple 3 is composed of a peralkaline and a peraluminous equivalent to the base composition (created by making up glasses with a defi-

**TABLE 2.** Experiment conditions and starting compositions

| Experiment | JMPC43 | JMPC46 | JMPC49 | JMPC51 | JMPC64 | | | JMPC41 | JMPC44 |
|---|---|---|---|---|---|---|---|---|---|
| Couple no. | 1 | 2 | 3 | 4 | 4 | | | 4 | 1 |
| $T$(°C) | 1300 | 1300 | 1300 | 1300 | 1300 | | | 1600 | 1600 |
| Time (s) | 6240 | 7080 | 7200 | 7860 | 3600 | | | 1920 | 1800 |
| Top | HPG3 | HPG2 | HPG8 + Al | HPG9 | HPG9 | $\sigma$ | C.V. (%) | HPG9 | HPG3 |
| $K_2O$ | 5.91 | 4.16 | 4.14 | 5.73 | 5.84 | 0.031 | 0.72 | 5.77 | 5.84 |
| $Na_2O$ | 4.54 | 5.50 | 5.09 | 3.56 | 3.56 | 0.034 | 0.63 | 3.57 | 4.58 |
| $Al_2O_3$ | 13.50 | 13.13 | 12.83 | 11.57 | 10.91 | 0.077 | 0.70 | 11.29 | 13.17 |
| $SiO_2$ | 73.15 | 73.91 | 75.54 | 76.51 | 76.28 | 0.100 | 0.13 | 76.38 | 73.90 |
| $H_2O$ | (2.90) | (3.30) | (2.40) | (2.90) | (3.40) | 0.040 | 1.33 | (2.95) | (2.51) |
| Bottom | HPG13 | HPG14 | HPG8 − Al | HPG7 | HPG7 | | | HPG7 | HPG13 |
| $K_2O$ | 2.66 | 4.19 | 4.10 | 2.63 | 2.59 | | | 2.57 | 2.61 |
| $Na_2O$ | 4.60 | 3.55 | 3.86 | 5.54 | 5.61 | | | 5.77 | 4.65 |
| $Al_2O_3$ | 9.98 | 9.61 | 9.98 | 11.57 | 11.13 | | | 11.32 | 9.72 |
| $SiO_2$ | 79.35 | 80.15 | 79.17 | 77.35 | 77.26 | | | 77.29 | 80.15 |
| $H_2O$ | (3.40) | (2.50) | (2.90) | (2.90) | (3.40) | | | (3.05) | (2.91) |

*Notes:* Compositions determined by EMPA and FTIR and recalculated to 100%, keeping water at the level established by FTIR. Water concentrations in parentheses are based on a small number of points for each side of couple, and were not used to fit diffusion profiles for water. Errors reported sigma are one standard deviation as calculated for homogeneity tests on zero-time (i.e., very short-duration) experiments; C.V. is coefficient of variation (standard deviation/mean).

ciency or excess, respectively, of 2.5 wt% $Al_2O_3$), whereas couple 5 is composed of the base composition itself in which one side contains approximately 2 wt% $H_2O$ and the other approximately 4 wt% $H_2O$ (Table 2), both crossing at HPG8 + 3% $H_2O$. A further two couples (6 and 7 in Table 2) consisted of the base composition on one side whereas the other side contained an additional 5 wt% of $Na_2O$ or $K_2O$. The bulk compositions of these two couples are offset slightly from those of the other five by about 2.5 wt% (relative) of each of the other components. No couple shows concentration differences of more than 6.5 wt% in any of the oxide components, to minimize the compositional dependence of [*D*]. Because our five-component composition space could theoretically be spanned by only four experiments, and our seven couples are at high angles to one another in composition space, we are confident that we have covered all possible orientations of the eigenvectors effectively.

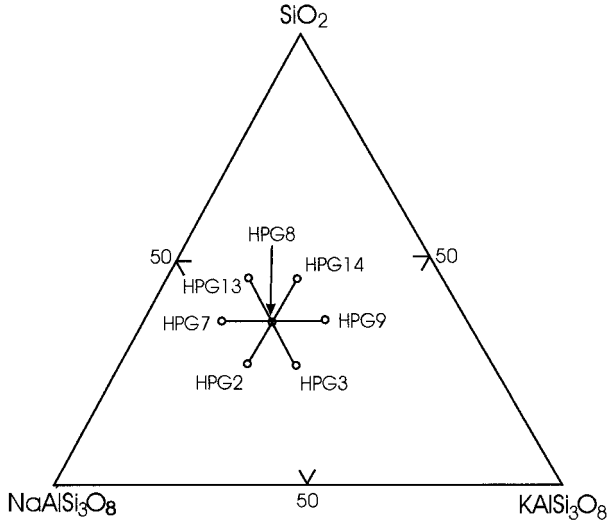


**FIGURE 1.** Positions of end-member compositions relative to the haplogranite plane. See text for descriptions of couples, listed also in Table 2.

### Analytical methods

Our experimental products were sawn in half longitudinally. One half was made into a polished thick section for EMPA, and the other half was cut and polished on both sides to 1000 μm thickness for measurement of water contents by Fourier transform infrared (FTIR) spectroscopy. EMPA data were collected as linear traverses containing between 100 and 500 data points for each experimental product. The FTIR data were affected somewhat by the large size of the analysis spot (100 μm) and the time involved in making each measurement, so that traverses contained fewer analyses. Therefore, we combined the data sets for oxides and for water by interpolating values of water content at each EMPA spot.

EMPA were obtained using a CAMECA SX-50 instrument; operating conditions were 15 kV accelerating voltage and 20 nA beam current, as measured with a Faraday cup. X-ray emissions were collected with four wavelength dispersive spectrometers over count times of 25 s for Al and Si, and 50 s for Na and K. Raw data were processed with a PAP correction program (Pouchou and Pichoir 1991). To prevent diffusion of Na and H away from the volume of glass activated by the electron beam, we used an expanded beam having a diameter of approximately 10 μm, which was swept along a line 100 μm long at a scan rate of approximately 25 μm/s. In this manner we were able to analyze water-rich and Na-rich glasses repeatedly on the same spot with minimal changes in composition. The scan line was oriented perpendicular to the direction of the analytical traverse, ensuring that the effective spot size along the direction of the traverse did not exceed the 25 or 50 μm spacing between analysis spots. Most products were analyzed over the entire length of the capsule, however a few EMPA traverses were cut off within 1000 μm of the ends of the capsules. In such cases, the remaining length was explicitly accounted for when required in finite couple solutions to the diffusion equation.

During quench of the experiments, transverse fractures commonly formed due to release of pressure related to

**TABLE 2—***Continued*

| Experiment | JMPC47 | JMPC50 | JMPC61 | JMPC95B | JMPC101 | JMPC102 |
|---|---|---|---|---|---|---|
| Couple no. | 2 | 3 | 5 | 2 | 6 | 7 |
| *T*(°C) | 1600 | 1600 | 1600 | 1600 | 1600 | 1600 |
| Time (s) | 1800 | 1800 | 360 | 1800 | 1260 | 1200 |
| Top | HPG2 | HPG8 + Al | HPG8 + H | HPG2 | HPG8 + Na | HPG8 + K |
| $K_2O$ | 4.14 | 4.15 | 4.00 | 4.12 | 3.93 | 9.79 |
| $Na_2O$ | 5.56 | 4.92 | 4.91 | 5.85 | 7.76 | 3.28 |
| $Al_2O_3$ | 13.13 | 12.59 | 10.81 | 13.18 | 11.05 | 11.60 |
| $SiO_2$ | 73.67 | 76.95 | 76.08 | 73.84 | 74.99 | 73.40 |
| $H_2O$ | (3.50) | (2.39) | 4.19 | 2.85 | 2.28 | 1.92 |
| Bottom | HPG14 | HPG8 − Al | HPG8 − H | HPG14 | HPG8 | HPG8 |
| $K_2O$ | 4.13 | 4.09 | 4.10 | 4.10 | 3.93 | 4.32 |
| $Na_2O$ | 3.71 | 4.26 | 5.21 | 3.76 | 5.65 | 5.42 |
| $Al_2O_3$ | 9.68 | 9.74 | 10.71 | 9.61 | 10.97 | 11.04 |
| $SiO_2$ | 80.07 | 78.97 | 77.78 | 79.29 | 77.22 | 76.98 |
| $H_2O$ | (2.41) | (2.95) | 2.19 | 3.25 | 1.95 | 2.24 |

**TABLE 3.** Absorptivities used in FTIR analysis for $H_2O$ and OH

| | HPG2 | HPG3 | HPG7 | HPG8* | HPG9 | HPG13 | HPG14 |
|---|---|---|---|---|---|---|---|
| $\epsilon_{H_2O}$ | 1.703 | 1.755 | 1.738 | 1.79 | 1.843 | 1.825 | 1.878 |
| $\epsilon_{OH}$ | 1.523 | 1.565 | 1.518 | 1.56 | 1.602 | 1.555 | 1.597 |

* Absorptivities for HPG8 + Al, HPG8 − Al, HPG8 + K, and HPG8 + Na all assumed equal to those for HPG8.

thermal contraction as the assembly was cooled rapidly. We measured the widths of these fractures and subtracted them from the analysis profiles.

The split of the experiment product intended for FTIR analysis was doubly ground to a thickness of 1000 μm using alumina abrasives followed by a final polish using diamond powder with water as the lubricant. Polished samples were cleaned with acetone to remove epoxy. The samples were then positioned over an aperture in a brass disk to aim a collimated beam at the sample. To decrease the spot size further, we introduced a brass slit between the aperture holes and the sample, which produced an effective spot size of 100 μm in a direction perpendicular to the line of traverse. A Bruker IFS 120 HR Fourier transform spectrophotometer was used to obtain transmission infrared spectra in the NIR region (2500–8000 $cm^{-1}$) using a W light source, a $CaF_2$ beamsplitter, and a narrow band MCT detector. The spectrophotometer operated at a resolution of 4 $cm^{-1}$ with a scanning speed of 20.0 kHz. A 32× cassegranian objective was used. Typically, 500–1000 scans were collected for each spectrum; background was recorded and subtracted in each case. The two bands of interest in the NIR region are at 4500 and 5200 $cm^{-1}$, attributed respectively to the combination stretching and bending modes of X-OH groups and of molecular water groups (Stolper 1982; Newman et al. 1986). For the band at 5200 $cm^{-1}$, a linear background tangent to the flanking minima was chosen; this background was extrapolated to lower frequency and used at 4500 $cm^{-1}$ also. The concentration of dissolved water in the glass contributing to a given band was calculated as the product of the molecular weight of water and the absorbance divided by the product of the sample thickness, the molar absorptivity (extinction coefficient), and the sample density (see Romano et al. 1995 for further details).

Because we measured water concentrations along profiles across inhomogeneous materials, the dependence of absorptivities for OH and $H_2O$ on composition was a matter of some concern. We considered the published values of molar absorptivities for compositions along the join Ab-Or (Romano et al. 1995; Behrens et al. 1996) and for haplogranitic glasses (Nowak and Behrens 1995), and both interpolated and extrapolated to each of the seven of our end-member compositions whose anhydrous equivalents lie within the haplogranite plane (Fig. 1). The estimated absorptivities are listed in Table 3. For couples whose end-members do not lie in the haplogranite plane, we used constant values of absorptivities equal to those measured for the base composition HPG8. Using this approach, we found that inferred absorptivities depend primarily on the $Al_2O_3$ content of the glass. Because the concentration of $Al_2O_3$ in all of our measured profiles is essentially a step function at the level of spatial resolution of the FTIR analyses, we treated each side of the annealed couple as homogeneous with respect to absorptivity, using the value we had adopted for the original end-member over the entire half-profile. Although the method of linear interpolation and extrapolation introduces some errors in derived water contents, it is probably more accurate than using a single set of absorptivities throughout the study. We also stress that in the example of experiment JMPC95B (Fig. 2c), the observed uphill diffusion of water is not an artifact of the adopted absorptivities because the shape of the profile remains qualitatively the same if a single set of absorptivities is used over the whole profile.

## RESULTS

### Diffusion profiles

The results of some of our experiments are presented in Figure 2 as concentration profiles. The complete data set is far too large to be presented here, even graphically. We have plotted the concentrations as mole fractions of the components $K_{12}O_6$, $Na_{12}O_6$, $Al_4O_6$, $Si_3O_6$, and $H_{12}O_6$. The six-O molecules were an arbitrary choice of component, which permit comparison with the only other published multicomponent diffusivities for granitoid melts (Chakraborty et al. 1995a, 1995b). It is important to note that once these arbitrary components have been chosen, the [*D*] that is extracted from the profiles is applicable only to these components. Clearly, expressing mole fractions with different stoichiometries leads to different nominal concentration differences and therefore requires different $D_{kl}$ to relate the fluxes to the concentration gradients.

Several qualitative features are immediately visible upon inspection of Figure 2. First, there are two different length scales of diffusion in the profiles. A long length scale, on the order of 1 cm in all cases, is associated with the long, gentle slopes in concentrations of alkalis and water (e.g., Figs. 2a, 2b, 2d, and 2e) and, in some cases silica (e.g., Figs. 2b and 2d). A much shorter length scale is associated invariably with the alumina concentration profiles, and this length scale is also observed in profiles of all other elements when there is an initial difference in alumina concentration across the couple (e.g., Fig. 2c). In other words, alumina diffusion is itself restricted to a very short length scale, and induces short length-scale effects on the otherwise much longer profiles of all the other components. Second, all of the profiles of the 1300 °C experiments can be superimposed upon the profiles of the 1600 °C experiments by a suitable linear transformation of the spatial scale, illustrated for selected profiles

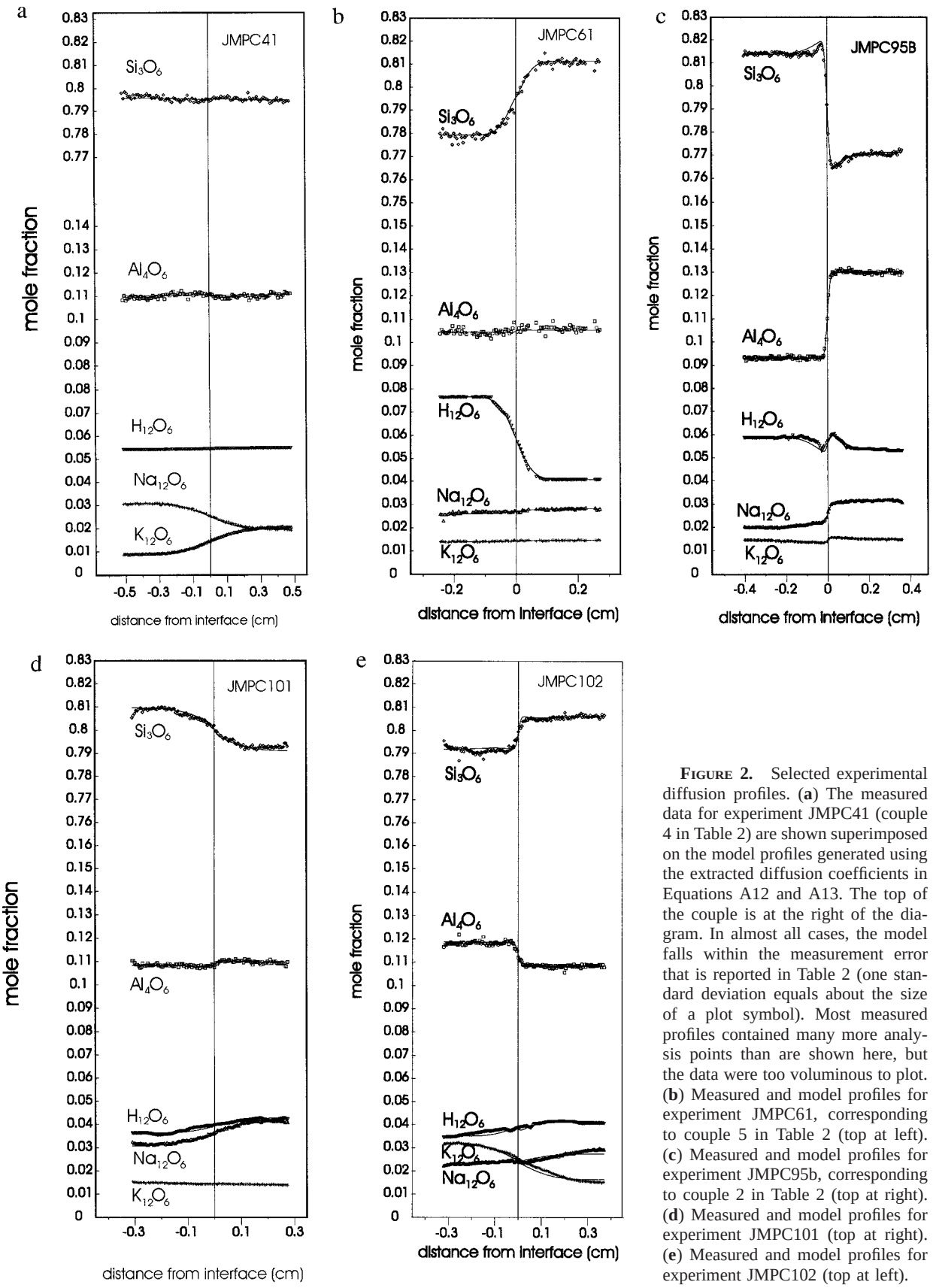


**FIGURE 2.** Selected experimental diffusion profiles. (**a**) The measured data for experiment JMPC41 (couple 4 in Table 2) are shown superimposed on the model profiles generated using the extracted diffusion coefficients in Equations A12 and A13. The top of the couple is at the right of the diagram. In almost all cases, the model falls within the measurement error that is reported in Table 2 (one standard deviation equals about the size of a plot symbol). Most measured profiles contained many more analysis points than are shown here, but the data were too voluminous to plot. (**b**) Measured and model profiles for experiment JMPC61, corresponding to couple 5 in Table 2 (top at left). (**c**) Measured and model profiles for experiment JMPC95b, corresponding to couple 2 in Table 2 (top at right). (**d**) Measured and model profiles for experiment JMPC101 (top at right). (**e**) Measured and model profiles for experiment JMPC102 (top at left).

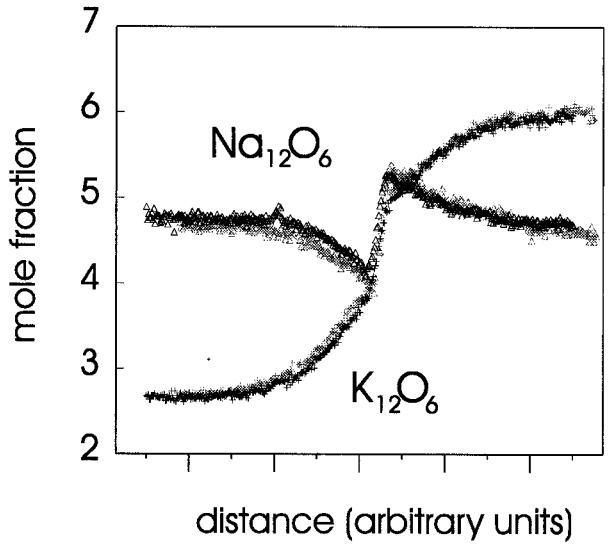


**FIGURE 3.** Measured profiles of JMPC44 (1600 °C) and JMPC43 (1300 °C). both along couple 1 in Table 2, superimposed by stretching the spatial scale of the two profiles (this process eliminates dependencies on both time and the eigenvalues), showing that they have obeyed the same set of eigenvectors. EMPA data for $K_{12}O_6$ are shown as crosses, whereas the data for $Na_{12}O_6$ are shown as triangles, plotted as solid symbols for JMPC44 and half-toned for JMPC43. The coincidence of the two profiles also shows that other mass transfer processes such as advection have not affected the forms of the profiles.

in Figure 3. The common trick of de-dimensionalizing the spatial scale with the Boltzmann variable (e.g., Crank 1975, p. 105) cannot be applied here because the two experiments were performed at different temperatures (i.e., the eigenvalues of [*D*] were different), so that the amount of stretching used to superimpose the two profiles does not contain any useful information. On the other hand, this superposition has two important implications. First, it can be used in place of the commonly employed time-series method to infer that the observed profiles are the result exclusively of diffusive processes, because distortions due to convection of the melt would not be expected to be reproduced between experiments with such different durations, temperatures, and viscosities. Second, it can be used to infer that the orientations of the eigenvectors of [*D*] did not change between 1300 and 1600 °C (or else the forms of the profiles would have changed).

To ensure that convection was not a source of error in our results, we performed two experiments of different duration (i.e., a time series) on one couple at 1300 °C. The time-series approach has important limitations that discouraged us from using it more widely. For the length of capsule we have used, there is a small window of useable experiment durations. For example, in experiments of longer duration, the longer length-scale profiles are finite and consequently increasingly poorly constrained due to the difficulties of controlling the shapes of the ends of the capsules. Similarly, in experiments of shorter duration, the shorter length-scale diffusion profiles become so short that there were too few data points in the sloping part of the profile to constrain the diffusivities. The only way to combat these difficulties would be to use longer capsules, but the experimental assembly requires that the capsules be no longer than the standard 11 mm capsule we used. Thus, one of the profiles had to be fit with the finite couple model equation, whereas the other was fit with the infinite couple equation; the [*D*] extracted using the shorter duration experiment could be used successfully to model the profile generated in the longer duration experiment.

### Water concentrations

Water concentrations were added to the EMPA data sets by taking spot analyses of water content and interpolating to produce estimated water concentration profiles. These interpolated profiles were then added to the EMPA data to produce a new data set that was normalized to 100%. Each microprobe analysis thus preserved the measured (or interpolated) water content at that point.

The water contents of several of the experiments were measured at only a few spots, because water contents were found not to have homogenized completely during the heating ramp at the beginning of the experiment. In these cases, water concentration profiles were not included in the $\chi^2$ analysis, but were used to constrain the concentrations of the other components by the recalculation described above. Although the uncertainty in water content in these experiments is much too large to permit extraction of components of [*P*] and [$\Lambda$] corresponding to water, it translates into a relative uncertainty in the recalculated concentrations of the other components of less than 1%, well within the error of the EMPA data. All determinations of components of [*P*] and [$\Lambda$] relating to water were performed on water concentration profiles from experiments JMPC61, JMPC95B, JMPC101, and JMPC102 (Figs. 2b–2e), which were prepared with prehydrated glasses to ensure homogeneity of the end-members of the couples at the commencement of the experiments.

### Diffusion coefficients

We used the interactive forward-modeling approach described above to fit the vector of eigenvalues and matrix of eigenvectors (Table 4) to the results of the experiments conducted at 1600 °C, using $Si_3O_6$ as the solvent. The eigenvalues are a fundamental property of the melt system and do not depend on the arbitrary choice of solvent, a property we have confirmed by repeating the fit using $Al_4O_6$ as the solvent (results not shown). The extended compositional vectors $\bar{\nu}^*$ derived with the two fits are identical.

The two largest eigenvalues we have determined, relating fluxes of K and Na to fluxes of other components, are degenerate within the precision of the microprobe data. As a result, there are no constraints on the K-Na and Na-K components of [*P*]; i.e., any value can be

**TABLE 4.** Eigenvectors, eigenvalues, and elements of [*D*]

| | $\nu_K$ | $\nu_{Na}$ | $\nu_{Al}$ | $\nu_H$ |
|---|---|---|---|---|
| | | | 0.096 | 0.17 |
| K | 1.00 | (0) | 0.076 | 0.00 |
| | | | 0.063 | −0.07 |
| | | | 0.225 | 0.22 |
| Na | (0) | 1.00 | 0.215 | 0.00 |
| | | | 0.195 | −0.32 |
| | 0.19 | 0.06 | | 0.23 |
| Al | (0.0) | −0.00 | 1.000 | −0.00 |
| | −0.15 | −0.26 | | −0.28 |
| | | | 0.38 | |
| H | (0) | (0) | 0.28 | 1.00 |
| | | | 0.15 | |
| $\nu^*_{Si}$ | −1.00 | −1.00 | −1.57 | −1.00 |
| | | **λ(×10⁻⁸ cm²/s)** | | |
| 1600 | 620 | 630 | 4.4 | 460 |
| | 550 | 540 | 3.4 | 280 |
| | 480 | 470 | 2.5 | 190 |
| 1300 | 220 | 260 | 0.45 | |
| | 190 | 240 | 0.34 | nd |
| | 160 | 210 | 0.25 | |

*Notes:* Eigenvector elements are expressed as triplets. Values from top to bottom of each triplet are upper bound, best fit, and lower bound, respectively, based on $\chi^2$ fits to diffusion profiles (one standard error).

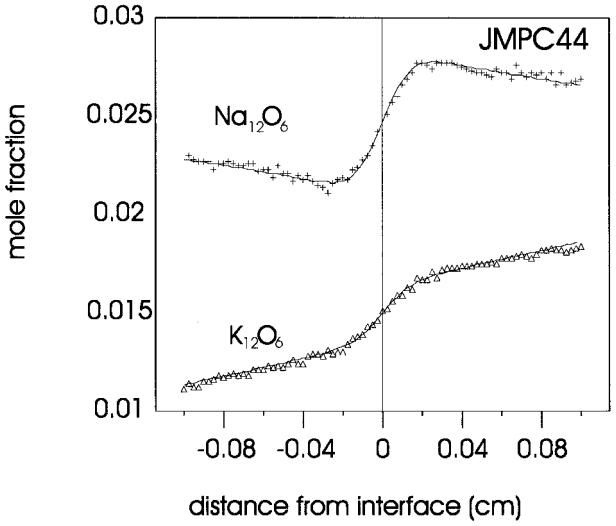


**FIGURE 4.** A detailed look at the central portion of JMPC44 (couple 1 in Table 2), showing all available data, displaying the quality of the fit to the subtleties of inflections in the measured profile.

placed in these elements of [*P*] and the resulting matrix can be used to provide an acceptable fit to the diffusion profiles. Because the K-Al and Na-Al, and the K-H and Na-H components of [*P*] are all found to have constraints (variations in these parameters leads to rejection of the model by the $\chi^2$ test), we conclude that the extended compositional vectors created from these two columns of the [*P*] matrix (see Eq. A17) lie within the ternary $Si_3O_6$-$K_{12}O_6$-$Na_{12}O_6$ plane. Therefore, all couples that show initial variations composed entirely of Na-K, Na-Si, and K-Si exchanges will show binary interdiffusion profiles with no observable coupling. A similar situation arises with respect to H-K, H-Si, and H-Na diffusion, as a result of the relatively poor analytical precision on the data for $H_{12}O_6$, despite the fact that the measured eigenvalue for $H_{12}O_6$ is significantly smaller than those of $Na_{12}O_6$ and $K_{12}O_6$. Therefore, all eigenvalues associated with Na, K, and H interdiffusion are effectively degenerate in the haplogranitic melt, to the degree of accuracy permitted by our EMP and FTIR analyses. More precise methods would permit separation of these nearly degenerate eigenvalues and observation of three distinct eigenvectors. However, we stress that the improved precision would have an insignificant effect on the shapes of profiles modeled using Equation A12. As a result of the degeneracy in the measured eigenvalues, a unique [*D*] matrix cannot be calculated for the hydrous haplogranitic system at the temperatures and pressure of our experiments. Substitution of any arbitrarily chosen value into [*P*] would generate one of an infinite number of very different looking [*D*], each of which would predict the forms of all of the diffusion profiles shown in Figure 2. It is for this reason that we report neither [*D*] nor errors in [*D*], but confine our attention to the matrix [Λ]. We remind the reader that [Λ] is a matrix of diffusion coefficients just like [*D*], and it can be used to predict interdiffusion of the chemical components whose stoichiometries are defined by the eigenvectors rather than the usual mole percent components with which we started our discussion.

The success of the fit to the data can be seen qualitatively by inspecting Figure 2, where the diffusion profiles predicted using Equation A12 for the eigen-parameters in Table 4 are shown as solid lines superimposed on the measured profiles. The model curves are with minor exceptions within the scatter of the data and duplicate in detail even subtle inflections in the experimental profiles. The quality of the fit for couple JMPC44 is illustrated in detail in Figure 4; the fits for most penetration profiles (other than those for water) were of similar quality. The misfit in $Si_6O_{12}$ observed in some profiles is a direct consequence of the relatively poor quality of the data for water because the recalculation of component concentrations to hydrous compositions places the greatest share of the distributed error onto $Si_6O_{12}$, the most abundant component.

The data collected on experiments conducted at 1300 °C suffer somewhat from the effects of irregularities in the polished surfaces of the sections due to the presence of quench-induced fractures. Despite these irregularities, we were able to fit a single [*P*] matrix to both the 1600 °C and the 1300 °C data sets. The only parameters that had to be fit differently for the results of experiments at these two temperatures were the eigenvalues [Λ].

## DISCUSSION

### Temperature dependence of [Λ]

In Figure 5 we show the relationship between the logarithms of the eigenvalues of [*D*] and reciprocal temper-

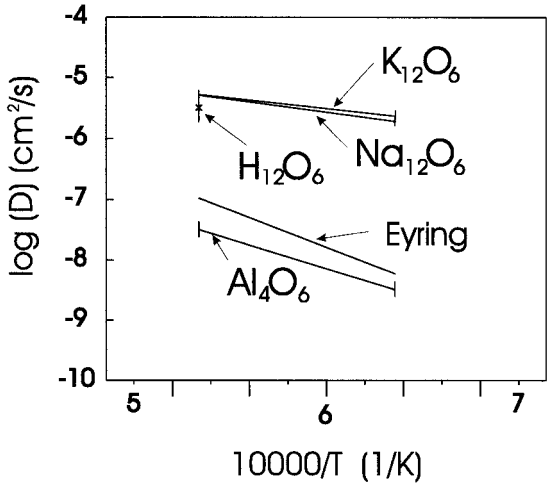


**FIGURE 5.** Arrhenius diagram showing logarithm of diffusion coefficients vs. reciprocal temperature. Note the effective equivalence (degeneracy) of the eigenvalues for $Na_{12}O_6$, $K_{12}O_6$, and $H_{12}O_6$-$Si_3O_6$ exchange. Also note that the diffusivity predicted for viscosity-controlling network formers by the Eyring equation is bracketed by the measured eigenvalues, but lies closest to the eigenvalue corresponding primarily to exchanges of $Al_4O_6$ for $Si_3O_6$. The error bars shown are one standard deviation, as reported in Table 4.

ature. Because we have data for only two temperatures, it is not possible to say whether the diffusivities show an Arrhenian dependence on temperature. We have also plotted the self-diffusivity of network-forming cations, $D^0$, as estimated from the Eyring equation:

$$D^0 = \frac{k_B T}{\eta \lambda^*} \quad (5)$$

(Glasstone et al. 1941), where $\eta$ is the melt viscosity, $k_B$ is Boltzmann's constant, and $\lambda^*$ is a length scale identified with the jump distance of a diffusive step. The Eyring equation is based on the premise that the diffusive jump whose length is represented by $\lambda$ is also the fundamental mechanism of viscous flow. We have chosen $5 \times 10^{-10}$ m for $\lambda^*$ (Mungall and Dingwell 1997) and have used an empirical model for viscosity of hydrous granitic melts to estimate $\eta$ (Hess and Dingwell 1996b). The diffusivity predicted by the Eyring equation is similar to that measured for the smallest eigenvalue in our experiments. Other investigators also have found a good correspondence between the predictions of the Eyring equation and experimentally derived diffusivities in silicate melts (e.g., Baker 1992; Lesher et al. 1996). We concur with the common suggestion (e.g., Chakraborty et al. 1995b) that the atomic-scale mechanism responsible for Al-Si interdiffusion, represented macroscopically in our results by the smallest eigenvalue, may exert a limiting control on the rate of viscous flow. Al makes up only about one-eighth of the tetrahedrally coordinated network-forming ions in the melt, but each Al ion is connected by T-O-T bonds to four other network formers. Thus, about half of the Si ions are members of Si-O-Al links, and consequently suffer a loss of mobility caused by the difficulty of breaking such links. If Al-O-Si linkages are much slower to break and reform than Si-O-Si linkages, the reactions involving Al would be expected to have a greater influence on the observed viscosity. In the limiting case of an infinitely slow Al-O-Si bond-breaking process, the Stokes-Einstein equation could be used with a particle size equivalent to that of a single $AlO_4$ tetrahedron surrounded by four $SiO_4$ tetrahedra. This case might relate well to the common observation that the Stokes-Einstein equation works well to relate viscosity to diffusivities in highly polymerized melts if the length scale chosen is about 10 times that used for the Eyring equation (cf. Mungall and Dingwell 1997).

Because $[\Lambda]$ is known at only two temperatures, it would be foolish to extrapolate our results to temperatures between the liquidus and the solidus of granitic magmas at upper crustal conditions. However, the similarity between the predictions of the Eyring equation and the smallest eigenvalue over the range of conditions reached in our experiments, suggests that there is great potential for the future prediction of $[\Lambda]$ through an extension of the Eyring equation to multicomponent liquids.

### Exchange vectors and transport mechanisms

In this section we discuss the implications of the eigenvectors for diffusive exchange processes. We define the locus in composition space of compositions described by a diffusion profile as the diffusion path (Gupta and Cooper 1971). If the orientation of the vector defined as:

$$\overline{C} = \overline{\chi}_1 - \overline{\chi}_2 \quad (6)$$

is parallel to an eigenvector, then the diffusion path is a straight line directly along the eigenvector. This corresponds to an exchange of chemical components that can be described entirely by the stoichiometry of the extended eigenvector $\overline{\nu}^*$. In other words, the extended eigenvector itself defines an exchange process in the melt. For example, the third eigenvector in the $[P]$ matrix extracted from our data using $Si_3O_6$ as the solvent has the extended vector:

$$\overline{\nu}^* = [(0.08_{K_{12}O_6}), (0.22_{Na_{12}O_6}), (1.00_{Al_4O_6}), (0.28_{H_{12}O_6}), (-1.57_{Si_3O_6})] \quad (7)$$

which corresponds to an exchange of $Al_4O_6$ and minor amounts of $K_{12}O_6$, $H_{12}O_6$, and $Na_{12}O_6$ for $Si_3O_6$. Because the identities of these exchanges do not change with a change of solvent, they are fundamental properties of the melt system that reflect processes, which can proceed independently of the fluxes of the other components. This definition of an exchange reaction is not consistent with that proposed by Chakraborty et al. (1995b), which does depend on the choice of solvent and consequently cannot be a fundamental melt property. During exchange along an extended eigenvector, each component appears to diffuse in a binary manner. This is the only situation in

which an effective binary diffusion coefficient (EBDC) corresponds to a diffusivity of general significance. The fact that along an eigenvector all components diffuse as though they were entirely independent of the other components, suggests that the stoichiometry of the extended eigenvector defines the average stoichiometry of the sum of all atomic scale processes, which combine to produce macroscopically observable fluxes.

If the orientation of a couple, $\overline{C}$, does not parallel an eigenvector, it must project onto at least two eigenvectors. The consequence of the orientation of $\overline{C}$ is that the erasure of the step change in concentration at the initial interface must proceed through the agency of at least two different exchange reactions, each of which proceeds at a different rate that is set by its eigenvalue. If the eigenvalues all have the same magnitudes, then the diffusion path will still be a straight line despite the fact that it does not parallel an eigenvector. The likelihood that one or more eigenvalues will be within measurement error of one another results in an important exception to the rule suggested by Trial and Spera (1994), who state that if a diffusion couple produces binary concentration profiles it must parallel an eigenvector. If the eigenvalues are different, then the more rapid exchange process will take place faster, causing the diffusion path closest to the endmembers to be deflected along the direction of the eigenvector associated with the larger eigenvalue and resulting in a non-binary looking profile.

The stoichiometries of the independent exchange reactions defined by our [*P*] matrix can be used to make qualitative inferences about the molecular-scale mechanisms for diffusive transport of the major element components of the melt. The simple, completely decoupled exchanges found for Group I oxides with silica imply that these exchanges do not affect neighboring Al ions at all.

It is has been suggested (e.g., Baker 1992) that alkalis exchange for one another within a relatively immobile lattice of tetrahedrally coordinated cations by a process that proceeds far more readily than any involving the tetrahedral sites themselves. We have shown that even though such alkali exchange is consistent with some of our results, equally rapid exchanges of alkalis for network-forming Si are required by the observed concentration profiles. It is tempting to argue that because a mechanism involving alkali-silica exchange is required to exist by the observations of silica-alkali diffusion, it is unnecessary and unjustified to propose an additional, extraneous mechanism for inter-alkali exchange.

The diffusion of water is thought to proceed by the formation of neutral water molecules that diffuse in a manner analogous to noble gases with minimal interactions with the other components of the melt (e.g., Wasserburg 1988). This hypothesis receives considerable support from the observation of infrared absorption attributed to the presence of $H_2O$ molecules (e.g., Shen and Keppler 1995). The operation of such a mechanism along the water-silica exchange eigenvector cannot be ruled out by our data, but the uphill diffusion of water linked to alumina-silica exchanges appears to result from coupling of dissociated water to alumina. For example, in experiment JMPC95B (Fig. 2c), the initial compositional profile for water was flat, and the interdiffusion of Al and Si led to the transfer of significant amounts of water across the interface. Furthermore, the identical diffusive behavior of all the Group I elements observed in our experiments strongly suggests that H, Na, and K are diffusing by the same set of mechanisms, and we are reluctant to propose the existence of free $Na_2O$ and $K_2O$ molecules in granitic melts. A possible way out of this dilemma is to propose that even though water can associate to form neutral molecules, such molecules may be forced to undergo a dissociation reaction to form their activated complex for diffusion (M. Nowak, personal communication). In this scenario, water molecules dissociate and migrate by a mechanism like that employed by alkalies, and rejoin to form $H_2O$ molecules again after the diffusive jump is complete. We could thus explain alkali metal and water diffusion by very similar mechanisms, while allowing for the existence of fully dissociated alkalis and both dissociated and molecular forms of water.

## Comparison to previous studies

### Water diffusion

Numerous studies have addressed the diffusion of water in granitic melts. The more rigorous treatments have modeled explicitly the extreme concentration dependence of the effective binary diffusivity of water at low concentrations (e.g., Karsten et al. 1982; Zhang et al. 1991). All previous studies of water diffusion have used couples like our couple 5 (experiment JMPC61), in which different amounts of water are present in a fixed base composition, in contrast to several other couples (e.g., couple 2, experiment JMPC95b), in which the response of water to fluxes of other components can be observed for the first time. Although the profile in Experiment JMPC61 does show some evidence for compositional dependence in the eigenvalue for water-silica exchange in the form of a distinct steepening at the lower concentrations, we have been able to neglect this effect because it is far less pronounced at the high water concentrations used in our study than it is in the case of hydration of an initially anhydrous glass or melt. In the direction of JMPC61, we observe pseudo-binary interdiffusion of water vs. a combined counterflux of alkalis and silica over a long diffusion region, but a short, sharp step in the alumina concentration. This result is due to the degeneracy of the eigenvalues for water- and alkali-silica exchanges; in other words, water exchanges for alkalis and silica whereas alumina remains relatively immobile. The short, sharp step in the modeled alumina concentration shown in Figure 2b is easy to overlook, particularly in experiments in which the total change in water concentration is on the order of 1 wt% or less,

allowing the common misconception that water diffuses independently of all other components in silicate melts. In fact, if one considers the implications of the diffusion equations, one realizes that it is impossible for a single component to diffuse entirely independently of other components except in the limiting case of true tracer diffusion (or the case in which all eigenvalues are equal). As we see in the profile for JMPC95b (Fig. 2c), an experiment in which water originally was present in equal concentrations on either side of the couple, but there was a gradient in alumina concentration, water is constrained to diffuse up its concentration gradient like the other Group I elements.

### Transient partitioning

It is interesting to compare the observed uphill diffusion with the concept of transient partitioning advanced by Watson (1982). He observed that $K_2O$ could diffuse uphill between basaltic and rhyolitic melts, leading to transient enrichments that persisted while slower-moving components retained appreciable gradients in concentration, and suggested that the effect resulted from large differences in activity coefficients in the two melt compositions. Similarly, if an experiment such as JMPC95B (Fig. 2c) were allowed to proceed for a much longer time than our experiment, the system would stabilize at some later time with elevated alkali and water contents in the alumina-rich side of the couple, despite having begun without any initial gradient in concentrations of either water or $Na_6O_{12}$. The partitioning, once established, would persist until the Al concentration gradient was erased by continued Al-Si interdiffusion. This type of transient partitioning is predicted by multicomponent diffusion theory for any couple not parallel to an eigenvector in which rapidly diffusing components show no initial concentration gradient. Although Watson (1982) attributed uphill diffusion to differences in activity coefficients between the two melts, this effect can be produced, in theory, by either kinetic factors, variations in activity coefficients, or combinations of both (e.g., Kuiken 1994).

### Eigenvector directions

Chakraborty et al. (1995b) measured eigenvectors in a multicomponent melt in the system $K_2O$-$Al_2O_3$-$SiO_2$ and found, as we did, that the exchange of alkalis for silica proceeds independently of alumina, whereas the exchange of alumina for silica always produces an associated flux of the alkali components. The eigenvectors for our five-component system project directly onto those of Chakraborty et al. (1995b) in the three-component subsystem, and we are able to predict the form of their diffusion profiles exactly using our eigenvectors along with their eigenvalues (J. Mungall, in preparation).

## Conclusions

In this study we have applied a theoretical model for chemical diffusion in multicomponent systems to experimental determinations of diffusion profiles in a synthetic analog to granitic melts. The results of our study indicate that the irreversible thermodynamic treatment for constant diffusion coefficients describes multicomponent diffusion in granitic magmas within the analytical uncertainty of EMP and FTIR analyses of melt compositions.

Inspection of the eigenvectors of the matrix of diffusion coefficients shows that alkalis and water diffuse through exchanges with silica, each of these exchanges being capable of proceeding independently of all others in the melt. In sharp contrast to this behavior, diffusive exchange of alumina for silica is found to cause concomitant fluxes of alkalis and water. The coupling of fluxes of alumina with fluxes of alkalis and water is likely to result from the need for $Al^{3+}$ in tetrahedral coordination in the melt to be charge-balanced by a nearby $M^{+}$ ion. The eigenvalue associated with alumina-silica exchange is approximately two orders of magnitude smaller than those associated with exchanges of alkalis and water for silica.

The eigenvectors of the diffusion matrix appear to be constant through large variations in temperature and composition, whereas the eigenvalues show strong temperature dependencies. Application of the Eyring equation to our base melt composition at the two temperatures at which we determined the multicomponent diffusion coefficients predicts a value somewhat smaller than the eigenvalue associated with alumina-silica exchange within experimental error, suggesting that alumina-silica exchange is the rate-limiting process in a viscous flow process involving exchanges of both $M^{1+}$ and Al for Si. The regularity of the relationship between the eigenvalues and the diffusivity predicted by the Eyring equation, together with the apparent constancy of the eigenvectors, holds promise for the eventual development of predictive models for multicomponent diffusion that would require melt viscosity as the only input parameter, over wide ranges of composition and physical conditions.

The extracted set of diffusion coefficients is general to all haplogranitic melts near the water-saturated eutectic at high temperatures and high pressures and should be of use to investigators interested in various processes including crystal growth, magma mixing, and viscous flow. The present work should be regarded as a first step toward a general investigation of the dependence of the eigenvectors and eigenvalues of $[D]$ on temperature, pressure, and melt composition, with the aim of deriving a predictive model for chemical diffusion in all natural silicate melts. Equipped with such a model, we will be able for the first time to make quantitative predictions of the role of rate processes in controlling a multitude of time-dependent igneous phenomena.

## Acknowledgments

This work was performed while J.E.M. held a NSERC postdoctoral fellowship on the visitor's program at the Bayerisches Geoinstitut. We thank Detlef Krause and Paddy O'Brien for their help on the microprobe, and Hubert Schulze for his expert preparation of polished sections. Don Baker and Frank Spera conducted thorough reviews that contributed greatly to the final manuscript.

## References cited


Allègre, C.J., Provost, A., and Jaupart, C. (1981) Oscillatory zoning: A pathological case of crystal growth. Nature, 294, 223–228.

Baker, D.R. (1992) Estimation of diffusion coefficients during interdiffusion of geologic melts: Application of transition state theory. Chemical Geology, 98, 11–21.

Behrens, H., Romano, C., Nowak, M., Holz, F., and Dingwell, D.B. (1996) Near-infrared spectroscopic determination of water species in glasses of the system $MAlSi_3O_8$ (M=Li, Na, K): an interlaboratory study. Chemical Geology, 128, 41–63.

Chakraborty, S. (1995) Diffusion in silicate melts. In Mineralogical Society of America Reviews in Mineralogy, 32, 411–504.

Chakraborty, S., Dingwell, D.B., and Rubie, D.C. (1995a) Multicomponent diffusion in ternary silicate melts in the system $K_2O$-$Al_2O_3$-$SiO_2$: I. Experimental measurement. Geochimica et Cosmochimica Acta, 59, 255–264.

———(1995b) Multicomponent diffusion in ternary silicate melts in the system $K_2O$-$Al_2O_3$-$SiO_2$: II. Mechanisms, systematics, and geological applications. Geochimica et Cosmochimica Acta, 59, 265–277.

Crank, J. (1975) The Mathematics of Diffusion, 414 p. Oxford University Press, New York.

Fisher, G.W. and Lasaga, A.C. (1983) Irreversible thermodynamics in petrology. In Mineralogical Society of America Reviews in Mineralogy, 8, 171–210.

Ghiorso, M.S. (1987a) Modeling magmatic systems: Thermodynamic relations. In Mineralogical Society of America Reviews in Mineralogy, 17, 443–465.

———(1987b) Chemical mass transfer in magmatic processes III. Crystal growth, chemical diffusion and thermal diffusion in multicomponent silicate melts. Contributions to Mineralogy and Petrology, 96, 291–313.

Glasstone, S., Laidler, K.J., and Eyring, H. (1941) The Theory of Rate Processes. McGraw-Hill, New York.

Gupta, P.K. and Cooper, A.R. (1971) The [D] matrix for multicomponent diffusion. Physica, 54, 39–59.

Haase, R. (1990) Thermodynamics of Irreversible Processes, 513 p. Dover Publications, Inc., New York.

Hess, K.-U. and Dingwell, D.B. (1996a) The influence of excess alkalis on the viscosity of a haplogranitic melt. American Mineralogist, 80, 297–304.

———(1996b) Viscosities of hydrous leucogranitic melts: A non-Arrhenian model. American Mineralogist, 81, 1297–1300.

Hofmann, A.W. (1980) Diffusion in natural silicate melts: a critical review. In R.B. Hargraves, Ed., Physics of Magmatic Processes, p. 385–417. Princeton University Press, New Jersey.

Holz, F., Behrens, H., Dingwell, D.B., and Taylor, R.P. (1992) Water solubility in aluminosilicate melts of haplogranitic composition at 2 kbar. Chemical Geology, 96, 289–302.

Karsten, J.L., Holloway, J.R., and Delaney, J.R. (1982 Ion microprobe studies of water in silicate melts: temperature-dependent water diffusion in obsidian. Earth and Planetary Science Letters, 59, 420–428.

Kirkpatrick, R.J. (1983) Kinetics of crystallization of igneous rocks. In Mineralogical Society of America Reviews in Mineralogy, 83, 321–398.

Kress, V.C. and Ghiorso, M.S. (1993) Multicomponent diffusion in MgO-$Al_2O_3$-$SiO_2$ and CaO-MgO-$Al_2O_3$-$SiO_2$ melts. Geochimica et Cosmochimica Acta, 57, 4453–4466.

———(1995) Multicomponent diffusion in basaltic melts. Geochimica et Cosmochimica Acta, 59, 313–324.

Kubicki, J.D., Muncill, G.E., and Lasaga, A.C. (1990) Chemical diffusion in melts on the $CaMgSi_2O_6$-$CaAl_2Si_2O_8$ join under high pressures. Geochimica et Cosmochimica Acta, 54, 2709–2715.

Kuiken, G.D.C. (1994) Thermodynamics of Irreversible Processes Applications to Diffusion and Rheology, 427 p. Wiley, New York.

Lasaga, A.C. (1982) Toward a master equation in crystal growth. American Journal of Science, 282, 1264–1288.

Lesher, C.E., Hervig, R.L., and Tinker, D. (1996) Self diffusion of network formers (silicon and oxygen) in naturally occurring basaltic liquid. Geochimica et Cosmochimica Acta, 60, 405–413.

Lesher, C.E. and Walker, D. (1991) Thermal diffusion in petrology. In J. Ganguly, Ed., Diffusion, atomic ordering, and mass transport: selected topics in geochemistry. Advances in physical geochemistry, 8, p. 396–451. Springer-Verlag, New York.

Liang, Y., Richter, F.M., and Watson, E.B. (1996) Diffusion in silicate melts: II. Multicomponent diffusion in CaO-$Al_2O_3$-$SiO_2$ at 1500°C and 1 GPa. Geochimica et Cosmochimica Acta, 60, 5021–5035.

Mungall, J.E. and Dingwell, D.B. (1997) Actinide diffusion in haplogranitic melts: effects of pressure, temperature and water contents. Geochimica et Cosmochimica Acta, 61, 2237–2246.

Newman, S., Stolper, E.M., and Epstein, S. (1986) Measurement of water in rhyolitic glasses: Calibration of an infrared spectroscopic technique. American Mineralogist, 71, 1527–1541.

Nowak, M. and Behrens, H. (1995) The speciation of water in haplogranitic glasses and melts determined by in situ near-infrared spectroscopy. Geochimica et Cosmochimica Acta, 59, 3445–3450.

Pouchou, J.-L. and Pichoir, F. (1991) Quantitative analysis of homogeneous or stratified volumes applying the model PAP. In K.J.F. Heinrich and D.E. Newbury, Eds., Electron Probe Quantitation, p. 31–36. Plenum Press, New York.

Press, W.H., Teukolsky, S.A., Vetterling, W.T., and Flannery, B.P. (1992) Numerical Recipes in Fortran, 963 p. Second Edition, Cambridge University Press, Cambridge.

Richter, F.M. (1993) A method for determining activity-composition relations using chemical diffusion in silicate melts. Geochimica et Cosmochimica Acta, 57, 2019–2032.

Romano, C., Dingwell, D.B., and Behrens, H. (1995) The temperature dependence of the speciation of water in $NaAlSi_3O_8$-$KAlSi_3O_8$ melts: an application of fictive temperatures derived from synthetic fluid inclusions. Contributions to Mineralogy and Petrology, 79, 1125–1134.

Shen, A. and Keppler, H. (1995) Infrared spectroscopy of hydrous silicate melts to 1000 °C and 10 kbar: Direct observation of $H_2O$ speciation in a diamond-anvil cell. American Mineralogist, 80, 1335–1338.

Sparks, R.S.J., Barclay, J., Jaupart, C., Mader, H.M., and Phillips, J.C. (1994) Physical aspects of magma degassing. In Mineralogical Society of America Reviews in Mineralogy, 30, 413–445.

Stolper, E. (1982) The speciation of water in silicate melts. Geochimica et Cosmochimica Acta, 46, 2609–2620.

Toramaru, A. (1991) Model of nucleation and growth of crystals in cooling magmas. Contributions to Mineralogy and Petrology, 108, 106–117.

Trial, A.F. and Spera, F.J. (1990) Mechanisms for the generation of compositional heterogeneities in magma chambers. GSA Bulletin, 102, 353–367.

———(1994) Measuring the multicomponent diffusion matrix: Experimental design and data analysis for silicate melts. Geochimica et Cosmochimica Acta, 18, 3769–3783.

Tuttle, O.F. and Bowen, N.L. (1958) Origin of Granite in the Light of Experimental Studies in the System $NaAlSi_3O_8$-$KAlSi_3O_8$-$SiO_2$-$H_2O$, 153 p. Geological Society of America Memoir, 74.

Wasserburg, G.J. (1988) Diffusion of water in silicate melts. Journal of Geology, 96, 363–367.

Watson, E.B. (1982) Basalt contamination by continental crust: some experiments and models. Contributions to Mineralogy and Petrology, 80, 73–87.

Zhang, Y., Stolper, E.M., and Wasserburg, G.J. (1991) Diffusion of water in rhyolitic glasses. Geochimica et Cosmochimica Acta, 55, 441–456.



Manuscript received May 19, 1997
Manuscript accepted February 5, 1998
Paper handled by Peter I. Nabelek


## Appendix

Recall from Equation 1 that:

$$\overline{J} = -\rho[D]\frac{\partial \overline{x}}{\partial y} \quad \text{(A1)}$$

It can be shown that the matrix $[D]$ is positive and semidefinite (e.g., Kuiken 1994, p. 223; Gupta and Cooper 1971), with the very useful result that it is diagonalizable and

has real, positive eigenvalues. The eigenvalues $\lambda_i$ are the $(n - 1)$ roots of the polynomial:

$$p(\lambda) = \det([D] - \lambda[I]) = 0. \quad \text{(A2)}$$

The homogeneous system of equations:

$$([D] - \lambda_i[I])\overline{v}_i = 0 \quad \text{(A3)}$$

can be solved for the $(n - 1)$ eigenvectors, $v_i$, each associated with an eigenvalue $\lambda_i$. There is an infinite number of possible magnitudes for each eigenvector, and we choose one by setting one of the elements equal to a convenient number, for example 1. The eigenvectors are all linearly independent, because one is not a multiple of another. If the eigenvectors of $[D]$ are assembled columnwise into a square matrix $[P]$, and we define a matrix $[\Lambda]$ whose diagonal elements are the corresponding eigenvalues of $[D]$, then:

$$[D] = [P]\cdot[\Lambda]\cdot[P]^{-1}. \quad \text{(A4)}$$

Insertion of A4 into A1, and left-multiplying the resulting equation by the operator $[P]^{-1}$, yields:

$$[P]^{-1}\cdot\overline{J} = -\rho[\Lambda][P]^{-1}\frac{\partial\overline{x}}{\partial y} \quad \text{(A5)}$$

$(n - l)$ flux equations in which the fluxes and concentrations are expressed in terms of new, transformed chemical components whose stoichiometries are given by the relation:

$$\overline{u} = [P]\cdot\overline{x}. \quad \text{(A6)}$$

The fluxes of these new components $\overline{u}$ are independent, thus allowing them to be calculated separately from one another, because $[\Lambda]$ is a diagonal matrix.

The elements of $[D]$, and hence either $[\Lambda]$ or $[P]$ (or both), must depend on composition (see Kuiken 1994, p. 225). If the elements of $[D]$ and their compositional dependencies are known, it is possible to solve Equation A5 using numerical methods. However, the compositional dependence of $[D]$ prevents the derivation of analytical solutions to Equation A5. In the trivial case, we observe that the elements of $[D]$ may be approximated constant values over sufficiently small variations in composition. In the second case, we consider the possibility that the orientations of the eigenvectors represented by $[P]$ remain constant in composition space, so that $[P]$ itself is constant.

In both the case of constant $[D]$ and of constant $[P]$ only, the matrix $[P]^{-1}$ can be placed within the partial derivative on the right hand side of Equation A5. The species conservation equation can be written:

$$\frac{\partial}{\partial t}(\rho\overline{x}) = -\frac{\partial\overline{J}}{\partial y}. \quad \text{(A7)}$$

Introducing $[P]^{-1}$ to both sides of Equation A7, with the fact that a constant $[P]^{-1}$ commutes with both partial derivatives in Equation A7 gives:

$$\frac{\partial}{\partial t}(\rho[P]^{-1}\cdot\overline{x}) = -\frac{\partial}{\partial y}([P]^{-1}\cdot\overline{J}). \quad \text{(A8)}$$

Combining Equations A5, A6, A7, and A8 and retaining the assumption of constant $[P]$, yields:

$$\frac{\partial\overline{u}}{\partial t} = \frac{\partial}{\partial y}\frac{[\Lambda]\partial\overline{u}}{\partial y} \quad \text{(A9)}$$

which is a set of $(n - l)$ uncoupled binary diffusion equations each in the form of Fick's second law for variable diffusion coefficients. For the second case above, with only $[P]$ held constant, these uncoupled equations can be solved numerically in a manner exactly analogous to the solution of a binary diffusion equation in which the diffusion coefficient is a function of composition or space (e.g., Crank 1975, Chapters 8 and 9). For the first case above, with both $[P]$ and $[\Lambda]$ constant, $[\Lambda]$ can be moved outside the partial derivative on the right hand side, leaving $(n - l)$ mutually independent diffusion equations, each with a constant diffusion coefficient $\Lambda_{kk}$.

The most popular experimental configuration in investigations of chemical diffusion is the couple, in which two reservoirs of melt with contrasting and initially homogeneous compositions $\overline{\chi}_1$ and $\overline{\chi}_2$ ($\overline{u}_1$ and $\overline{u}_2$ in the transformed compositions) are brought into contact along a planar interface at zero time and allowed to interdiffuse for a known period of time before quenching. This geometry approximates well to a one-dimensional system if the two reservoirs have matching sides perpendicular to the interface, or at large distances from the container walls if the walls are irregular. If measurable diffusive fluxes do not reach to the ends of the two reservoirs, they are effectively infinite in extent, and the couple is called an infinite couple. If the fluxes do affect compositions at the ends of the reservoirs then the couple is called a finite couple.

Following Gupta and Cooper (1971) and Trial and Spera (1994), we write a general solution to Equation A9 for constant $[\Lambda]$ in the form:

$$\overline{u} = \frac{\overline{u}_1 + \overline{u}_2}{2} + [F](\overline{u}_1 - \overline{u}_2) \quad \text{(A10)}$$

where $[F]$ is a diagonal linear operator whose diagonal elements are functions of time, space, and the eigenvalues of $[D]$. Then:

$$\overline{x} = \frac{\overline{\chi}_1 + \overline{\chi}_2}{2} + [P]\cdot[F]\cdot[P]^{-1}\cdot(\overline{\chi}_1 - \overline{\chi}_2) \quad \text{(A11)}$$

or in expanded form:

$$x_k = \frac{\chi_{k(1)} + \chi_{k(2)}}{2} + \sum_{l=1}^{n-1}\sum_{m=1}^{n-1} P_{kl}F_{lm}P^{-1}_{lm}\Delta x_m. \quad \text{(A12)}$$

For the infinite couple:

$$F_{lm} = \frac{1}{2}\delta_{lm}erf\left(\frac{y}{\sqrt{4\Lambda_{lm}t}}\right) \quad \text{(A13)}$$

and for the finite couple:

$$F_{lm} = \frac{2}{\pi}\delta_{lm}\sum_{n=1}^{\infty}\left[\frac{1}{n}\cos\left(\frac{n\pi(L_1 + y)}{L_1 + L_2}\right) \times \sin\left(\frac{n\pi L_1}{L_1 + L_2}\right)e^{-n^2\pi^2\Lambda_{lm}t/(L_1+L_2)^2}\right] \quad \text{(A14)}$$

where $L_1$ and $L_2$ are the lengths of the two sides of the couple

(Trial and Spera 1994). If $L_1$ and $L_2$ are not equal, then the first term on the right hand side of Equations A11 and A12 (the bulk composition of the couple) is redefined as:

$$\overline{\chi}_{\text{bulk}} = \frac{L_1}{L_1 + L_2}\overline{\chi}_1 + \frac{L_2}{L_1 + L_2}\overline{\chi}_2. \quad \text{(A15)}$$

The finite couple solution is appropriate when the following condition is satisfied:

$$\frac{\Lambda_{lm} t}{(L_1 + L_2)^2} < 10^{-2} \quad \text{(A16)}$$

(Trial and Spera 1994).

As Trial and Spera (1994) pointed out, the eigenvectors depend on the choice of solvent. However the underlying diffusive coupling described by the eigenvectors must be invariant with choice of solvent, because the solvent choice is an arbitrary matter. Similarly, the identities of the $(n - l)$ independent eigenvalues must also be invariant with the choice of solvent. A solvent-independent set of vectors in the composition space, each associated with one of the eigenvalues, can be derived from a particular set of eigenvectors as follows. The new vector $\overline{v}^*$ consists of the original $(n - 1)$ elements of the eigenvector and an additional, $n^{\text{th}}$ element, which is defined as:

$$v_n^* = -\sum_{k=1}^{n-1} v_k \quad \text{(A17)}$$

so that the sum of all of the elements of the new vector is zero. The vectors $v$ so defined all lie within the surface including the $n$ compositions $\overline{\chi}_k = (1, 0, \ldots 0)$, $\overline{\chi}_{k+1} = (0, 1, 0 \ldots 0) \ldots \overline{\chi}_n = (0 \ldots 0, 1)$. In a ternary system, this plane corresponds to the ternary diagram familiar to petrologists.